Calculated Raman Optical Activity Spectra of 1,6-Anhydro-β-D-glucopyranose

Sandra Luber and Markus Reiher*

Laboratorium für Physikalische Chemie, ETH Zürich, Wolfgang − Pauli-Str. 10, CH-8093 Zürich, Switzerland

Received: March 29, 2009; Revised Manuscript Received: June 5, 2009

We present calculations of Raman and Raman optical activity spectra of the carbohydrate molecule 1,6-anhydro-β-D-glucopyranose. It is shown that a change from the chair to the boat conformation has a strong influence on the calculated Raman optical activity intensities. Similar results are found for different rotamers of this molecule. In order to investigate solvent effects, we perform calculations with and without the continuum model COSMO. In addition, explicit solvation with water molecules is investigated, and is shown to significantly affect the calculated Raman optical activity spectrum. The final spectra are constructed by overlaps of spectra of single conformers leading to a good agreement with the experimental spectra.

1. Introduction

Anhydro sugars are sugar derivatives which formally emerge by water elimination of aldoses and ketoses. Their reactivity depends on the size of the cyclic sugar structure,[1] and they are utilized as starting reagents for different types of syntheses, which do not necessarily involve only carbohydrate molecules. In 1917, the very first anhydro sugar was discovered, namely for the molecule D-*altro*-heptulose.[2] Another example of an anhydro sugar is 1,6-anhydro-β-D-glucopyranose (AGP), which can be formed by dry distillation of D-glucose.[3] Aqueous acid leads easily to hydrolysis of this anhydro sugar to glucose,[4] which makes it a valuable reagent for, e.g., the preparation of glucose derivatives and polymerization reactions.[3,5]

When D-glucose is treated with aqueous acids, the resulting equilibrium mixture contains AGP only in small amounts so that it remained undiscovered for a long time.[6] Nevertheless, nuclear magnetic resonance,[7−9] kinetic,[10] and optical rotation[11,12] experiments as well as molecular mechanics simulations[13,14] have been performed, demonstrating that the $^1C_4$ chair conformation is the dominant conformation. It was also found in crystal structures.[3,15] Furthermore, a Raman optical activity (ROA) spectrum[16,17] was published in 1991.[18] Since the interpretation of this spectrum is not completely obvious, calculations can provide a deeper understanding of the relationship between molecular vibrations and bands occurring in the ROA spectrum. ROA calculations for molecules of this size are nowadays feasible with contemporary computational methodology (for examples of ROA calculations, see refs 19−34). Although experimental data of carbohydrate molecules are available,[35−41] to our knowledge only one theoretical investigation of such ROA spectra has been published[42] dealing with glucose, lactose, and galactose derivatives. In that study, it was shown that the conformational flexibility of the sugar molecules and solvent effects have to be explored in order to obtain calculated spectra agreeing well with the experimental ones. As a consequence, the number of structures to be considered is in principle quite large already for these small molecules, but it can be significantly reduced by dealing solely with the low-energy conformers. Here, we study the ROA spectrum of AGP, which is a relatively rigid molecule. We examine the conformers of AGP for the chair and boat conformations, which results in 54 different structures.

This paper is organized as follows: after the computational methodology in section 2, the influence of the conformation and solvent effects are examined in section 3. The conformer populations as well as Raman and ROA spectra, constructed by overlaps of conformer spectra, are discussed in section 4 and compared to the experimental ones. The results are summarized in section 5.

2. Computational Methodology and Notation

Molecular structure optimizations were performed with Turbomole[43] employing density functional theory with the density functional BP86[44,45] and Ahlrichs' TZVPP basis set.[46,47] All vibrational spectroscopy calculations were carried out in the harmonic approximation with Snf.[48] It is well-known that harmonic BP86 vibrational frequencies match experimental fundamental ones very well[49−51] (see also the references in refs 52 and 53). This is a particularly useful error compensation as to include corrections for anharmonicity via perturbation theory[54] is very demanding in terms of computational effort and may fail in the case of Fermi resonances.

Gibbs enthalpies were calculated with Snf[48] in the particle-in-a-box-rigid-rotor-harmonic-oscillator approximation employing the same density functional and basis set as for the structure optimizations. Although this standard approximation is not particularly well suited for obtaining Gibbs enthalpies in condensed phase, we may assume that the approximation is sufficient, mostly because the translational and rotational partition functions hardly matter for the entropy in this approximation since all molecular comparisons rely on a constant number of particles (one molecule at a time), and hence these contributions basically drop out because of the equal masses and very similar moments of inertia. Because of the fact that Gibbs free enthalpies are approximated in such a way in standard quantum chemical calculations, we also rely on the pure electronic energy differences (i.e., at 0 K and without any corrections for nuclear motions) in our population analysis of different sugar conformations.

Snf[48] was also utilized for the calculation of the ROA spectra based on property tensors calculated for distorted structures from which all derivatives are obtained numerically. These polarizability tensors were evaluated with our local version of the escf

* To whom correspondence should be addressed. E-mail: markus.reiher@phys.chem.ethz.ch. Fax: +41-44-63-31594. Tel: +41-44-63-34308.

10.1021/jp902828r CCC: $40.75
Published on Web 07/01/2009

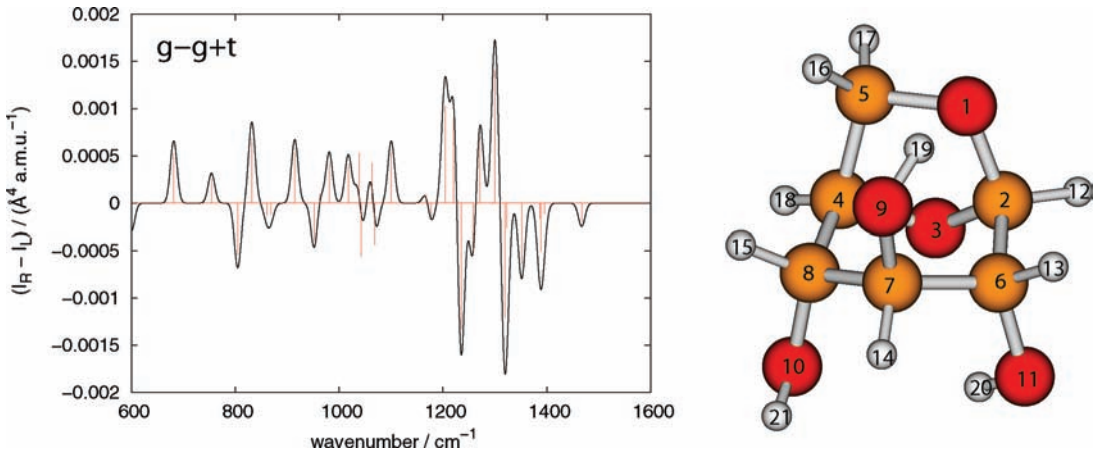

Figure 1. The optimized (TZVPP/RI/BP86) structure of the g−g+t conformer of AGP in the chair conformation (right-hand side) and the corresponding backscattering ROA spectrum (TZVPP/RI/BP86; left-hand side); the line spectrum was scaled by a factor of 0.05.

module of Turbomole[33] and are given as polarizability volumes, e.g., for the electric-dipole−electric-dipole polarizability we have $\alpha_{ij,V} = \alpha_{ij}/(4\pi\varepsilon_0)$, so that the ROA intensities are calculated in the units of Å^4/a.m.u. The excitation wavelength was set to 514.5 nm. We present only ROA spectra for the backscattering experimental setup, which are plotted with a Gaussian bandwidth of 15 cm^{-1}. Hence, the total ROA intensity of a vibration is broadened to simulate the effect of an environment in such a way that the integration over the band yields the calculated total ROA intensity. Consequently, after this artificial line broadening the units should be Å^4/(a.m.u.·cm^{-1}) though we stick to the usual convention and keep Å^4/a.m.u. as units keeping in mind that the full area of a band is referred to. The resolution-of-the-identity density-fitting technique[55] was exploited in all calculations.

Solvation is essential for polar functional groups as present in sugar molecules, but it is also the most difficult effect to model in calculations. For the calculation of vibrational spectra we require a reliable, but also efficient solvation model. Continuum solvation is a first step toward this. As a continuum model, we employed COSMO[56] with the standard settings as implemented in Turbomole. It can be anticipated that such a model is not well suited if directed weak contacts (hydrogen bonds) are built up from solvent molecules to the solute molecule, and hence microsolvated solute structures are an essential part of the modeling process (see, e.g., ref 57 for a detailed study of water-microsolvation of a solute molecule). The optimum quantum-chemical model is then a combination of continuum- and microsolvation. It is important to note that continuum solvation effects are not incorporated in the calculation of the property tensors, but they indirectly influence the Raman and ROA intensities via the COSMO-modified normal modes. They also affect the relative energies of conformers, their molecular structures, their vibrational frequencies and thus also the Gibbs enthalpies.

In principle, each hydrogen atom of the hydroxyl groups of AGP has several possibilities to orient themselves with respect to the ring. We consider gauche (g+ and g−, respectively, depending on the sign of the torsional angle) and trans (t) orientations. This orientation is described by dihedral angles, which we define as H(20)−O(11)−C(6)−C(2) for hydrogen atom H(20), H(19)−O(9)−C(7)−C(6) for H(19), and H(21)−O(10)−C(8)−C(4) for hydrogen atom H(21) (see Figure 1 for the numbering of the atoms). The conformations are denoted by an abbreviation, in which the first part refers to the dihedral angle corresponding to hydrogen atom H(20), the second one referring to H(19), and the last one to H(21). For example, g+g−t denotes the conformation with a positive gauche dihedral angle of H(20), a negative gauche torsional angle of H(19), and a trans dihedral angle of H(21).

3. Influence of Conformation and Solvent

In the following, we demonstrate how different conformations and solvent effects can influence the ROA intensities.

3.1. Chair versus Boat Conformation. First, we examine the differences in the ROA intensities for the $^1C_4$ chair and the $B_{0,3}$ boat conformation, where the numerals indicate the atoms which are located outside the chosen reference plane (for details about the notation, see ref 58). As an example, the ROA spectra of the chair and boat conformation of the g−g+t rotamer are given in Figures 1 and 2, respectively. In the spectrum of the chair conformation, the band at 681 cm^{-1} corresponds to a bending vibration, mainly of the ring atoms, and the negative band at 805 cm^{-1} to a C−C stretching vibration followed by a deformational vibration of the whole molecule at 832 cm^{-1}. A mixture of C−C stretching and deformational vibrations of the hydrogen atoms gives rise to the positive peak at 914 cm^{-1} and mainly deformational vibrations of the methylene groups of the ring lead to the negative band at about 950 cm^{-1}. The vibration at 981 cm^{-1} contains some stretching vibrations of the C(4) and O(3) atoms as well as deformational vibrations. Each band at 1018, 1039, and 1042 cm^{-1} involves a C−O stretching vibration of one of the three hydroxyl groups, respectively. The following intense bands involve deformational vibrations, mainly of the hydrogen atoms, in different variants. The normal mode at 1178 cm^{-1}, for example, includes a large movement of the H(21) hydrogen atom, while the negative one at 1319 cm^{-1} features bending especially of the H(21) and H(14) hydrogen atoms, and the other negative mode at 1351 cm^{-1} shows mainly bending of the H(19) hydrogen atom.

The ROA spectrum of the boat conformation of the g−g+t rotamer (compare Figure 2) agrees partly with the one of the chair conformation. This is most obvious in the region up to 1100 cm^{-1}, in which the intensity values differ, but the signs are (mostly) the same. In addition, some vibrations are shifted to higher wave numbers, but the corresponding bands of the ROA spectrum of the chair conformation can be assigned. Significant differences are observed at higher wave numbers. The strong negative bands at around 1150−1220 cm^{-1} were not found in the spectrum of the chair conformation, only a few weak ones. These normal modes are again bending

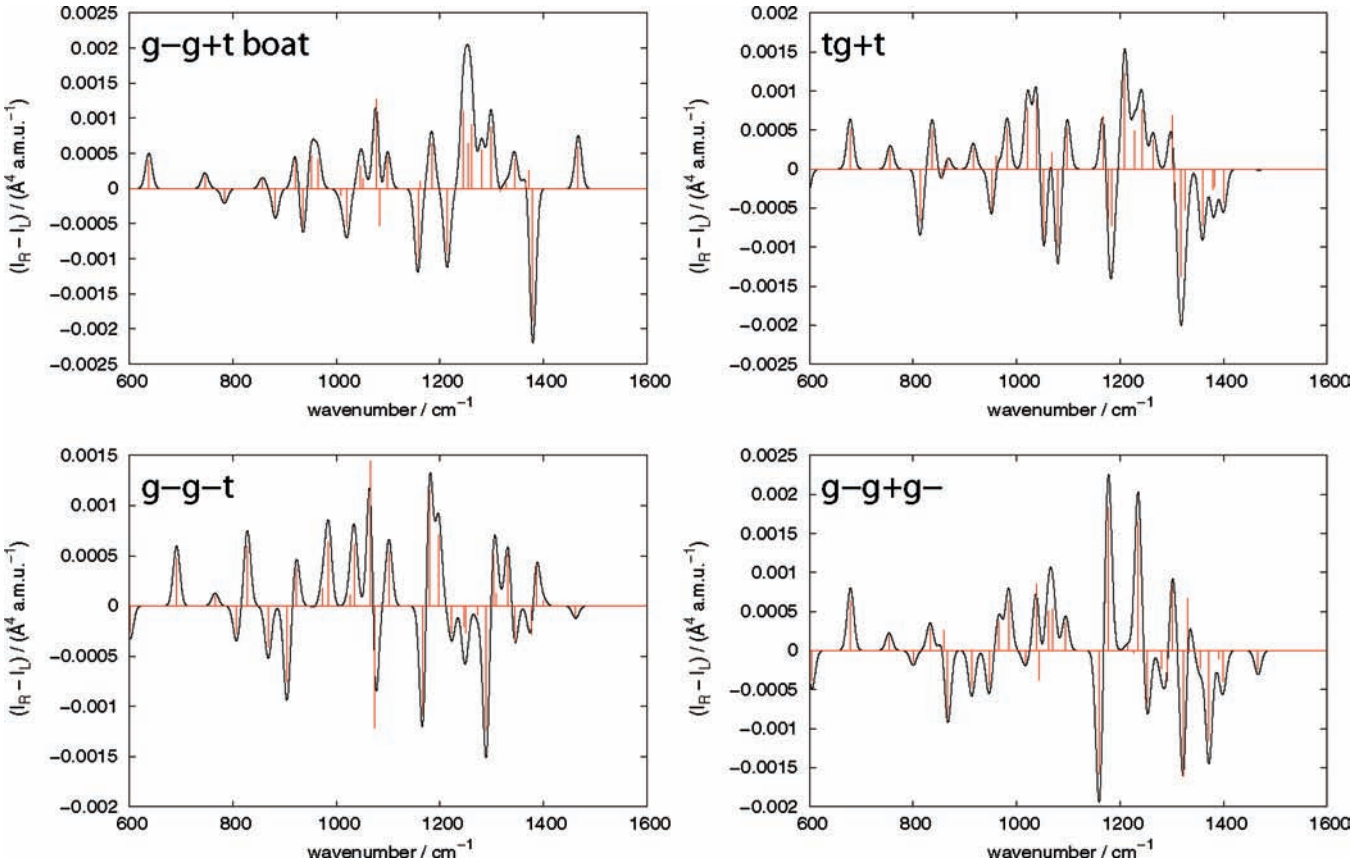

Figure 2. Calculated backscattering ROA spectra (TZVPP/RI/BP86) of AGP in the tg+t (right-hand side of the upper part), g−g−t (on the bottom at the left-hand side), and g−g+g− (on the right-hand side of the lower part) rotamers in the chair conformation and of the g−g+t (left-hand side of the upper part) rotamer in the boat conformation; the line spectra were scaled by 0.05.

vibrations, particularly of the hydrogen atoms. The intense negative peak at about 1379 cm^{-1} also corresponds to a bending mode, which involves especially the hydroxyl group at C(8). Worth mentioning are the different signs of the band at around 1450 cm^{-1}. It is negative in the case of the chair conformation and positive for the boat conformer. The underlying normal mode is a bending vibration of the two hydrogen atoms H(16) and H(17) of the methylene group in the ring. Although the motion of the atoms is quite similar, the corresponding intensities differ in sign since the magnetic-dipole containing invariant, the so-called $\beta(\mathbf{G}')$ invariant, in the intensity formula (for details about ROA theory, see e.g. ref 59) shows either a large positive or negative contribution for the boat and chair conformations, respectively, whereas the other invariant containing electric-quadrupole contributions is small. We performed a local decomposition according to the proposal of Hug[60] and found that the H(17) hydrogen atom always gives a negative contribution to the $\beta(\mathbf{G}')$ invariant, which is the dominant one in the chair conformation. However, in the boat conformation, the H(16) hydrogen atom and its coupling to the H(17) and C(5) atoms contribute a large positive amount so that the $\beta(\mathbf{G}')$ invariant and the overall intensity are positive. This demonstrates how difficult it is to understand the origins of ROA intensities.[61−63]

3.2. Influence of the Orientation of the Hydrogen Atoms in Hydroxyl Groups. As mentioned above, the hydrogen atoms of the hydroxyl groups can assume many different orientations since they can rotate almost freely. In the case of sugar molecules, the most common orientations are the gauche and trans orientations. Several spectra of conformers differing in this regard are shown in Figure 2.

The tg+t rotamer differs from the g−g+t rotamer by the orientation of the H(20) hydrogen atom. The corresponding spectra are very similar in the lower wavenumber region, in which mainly vibrations involving the carbon atoms occur. The largest differences occur at around 1200 cm^{-1}, where an intense negative peak is found for the tg+t conformer, whereas such a band occurs at about 1235 cm^{-1} in the spectrum of the g−g+t rotamer.

Changing the orientation of the H(19) hydrogen atom from a positive to a negative gauche torsional angle, the g−g−t conformer is obtained. Comparing its spectrum in Figure 2 to the one of the g−g+t rotamer (Figure 1), a similar pattern is found from 600 to 900 cm^{-1}. However, the positive and negative bands between 900 and 1000 cm^{-1}, which correspond to a mixture of stretching and deformational vibrations, show a reversed sign. The most conspicuous differences are again observed for the region from about 1150 to 1400 cm^{-1} since mainly hydrogen deformational vibrations occur in this range. Around 1200 cm^{-1}, several ROA intensities differ significantly and sign inversions lead to a different appearance of the spectrum from 1250 to 1400 cm^{-1}.

The ROA spectra are also sensitive to changes of the orientation of the H(21) hydrogen atom. This is demonstrated in Figure 2 for the g−g+g− conformer in comparison to the ROA spectrum of the g−g+t conformer (Figure 1). Significant differences are already detected for wave numbers higher than 900 cm^{-1}, although some similarities can be found in the peak pattern from about 1300 to 1400 cm^{-1} since the sign of the intensities are the same although the absolute values are different. Without going into more detail, it can be easily seen that already small changes in the orientation of the hydrogen atoms of the hydroxyl groups have a large effect on the ROA intensities.

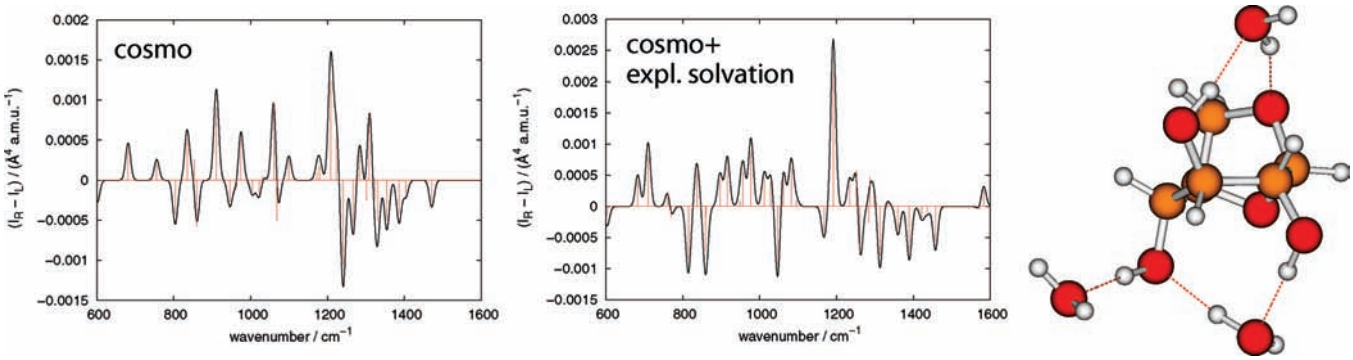

Figure 3. Calculated backscattering ROA spectra (TZVPP/RI/BP86) of the g−g+t conformer of AGP in the chair conformation obtained by employing the continuum model COSMO (left-hand side) and by explicit solvation with water molecules and COSMO (middle); the line spectra were scaled by 0.05. The optimized (TZVPP/RI/BP86) structure of the explicitly solvated g−g+t conformer is shown on the right-hand side.

3.3. Solvent Effects. We investigated two approximations in order to include solvent effects. The first one is the application of the COSMO continuum model which affects the energy, the molecular geometry and the molecular Hessian (i.e., vibrational frequency) calculation, whereas no COSMO corrections were included in the coupled-perturbed Kohn−Sham equations for the calculation of the property tensors. In Figure 3, the ROA backscattering spectrum of the g−g+t conformer is presented as obtained using COSMO. There are only small differences compared to the spectrum calculated without any solvent (see Figure 1). The values of the intensities differ, which is especially obvious for the large negative band at about 1300 cm^{-1}. In contrast to this, the changes in the wave numbers are small, and the overall pattern is thus quite similar. However, also a few sign changes are observed, particularly in the region from 1000 to 1050 cm^{-1}, which correspond to C−O stretching vibrations of the hydroxyl groups, and for the small peak at about 1180 cm^{-1}. However, the most remarkable pattern of the spectrum is not influenced by the intensities with reversed sign. Hence, the influence of the COSMO model is in total quite small compared to the spectrum calculated without the continuum model.

As a second approximation, we employed the continuum model and, in addition, solvated each hydroxyl group with one water molecule in such a way that the hydrogen atoms of the hydroxyl groups interact with the oxygen atoms of the water molecules (see Figure 3). There are many changes compared to the spectrum obtained solely with COSMO although the shifts in the wave numbers are small for the comparable normal modes. Even in the low wavenumber region, in which the skeletal vibrations occur, remarkable differences exist. For instance, the only positive band at about 700 cm^{-1} in the spectrum without water molecules splits into two positive bands involving stretching vibrations of, e.g., the C−O bonds in the rings, affecting the water molecule interacting with the H(19) hydrogen atom. The negative-positive-negative bands between 815 and 859 cm^{-1} show distinct intensities since they also involve the water molecules through some deformational vibrations of the hydroxyl groups. In the region between 900 and 1000 cm^{-1}, only positive bands are observed in contrast to the spectrum without solvent molecules, demonstrating the large influence of the water molecules on the intensities. All vibrations at higher wave numbers are more or less strongly modified due to the presence of the water molecules. Interestingly, the small positive peak around 1180 cm^{-1} in the spectrum obtained with COSMO and no explicit solvation is changed to a negative one if the water molecules are present and thus shows again the same sign as in the spectrum calculated without any solvent effect (Figure 1). In contrast, the intense positive mode at around 1200 cm^{-1} is found in all spectra whether or not solvent effects are incorporated.

4. Comparison of Calculated and Experimental Spectra

In this section, we present Raman and ROA spectra which are constructed from the calculated spectra of the different conformers. Since the conformers are usually not equally stable, we first examine their populations at room temperature.

4.1. Populations of the Conformers. First, we optimized all structures in the chair conformation without considering solvent effects. Minima were found for the conformers listed in Table 1. The one with the lowest electronic energy is the g−g+t conformer, which is shown in Figure 1, followed by the tg+g+ and tg−g+ conformers with an about 2 kJ/mol higher electronic energy than the g−g+t conformer. A slightly higher electronic energy was found for the g−g+g− rotamer. Considering also the g−g+g+ and g+g+g+ rotamers, which are about 4 kJ/mol higher in electronic energy, these six conformers represent about 95% of the total population evaluated by a Boltzmann distribution. Considering the Gibbs enthalpy (evaluated for a temperature of 298.15 K), the results are similar, although the most stable one is now the g−g+g+ rotamer, followed by the g−g+t rotamer. The Gibbs enthalpy differences are not so large for the six mentioned conformers as the electronic energy differences, but, nevertheless, their population sums up to about 73% of the total population. The remaining 27% mainly correspond to ten conformers contributing between 1.6 and 3.0% (see Table 1). The g−g+t conformation has already been determined to be the most abundant one by employing Gibbs energy differences from molecular mechanics simulations,[14] which may be due to favorable hydrogen bonding interactions of H(20) and H(19) with the oxygen atoms of the rings.

Interestingly, the second most abundant conformation was found to be the g−g−t conformation in ref 14, which is not the case in our calculations. However, the tg+g+ conformer, which Straathof et al. noted to be the one with the third highest population,[14] is also found in our calculations with a high population. Furthermore, they found the g−g+g−, tg−g+, and g+g+g+ conformations with population fractions of 6.6%, 6.1%, and 3.6%, respectively, which are in general lower than our population fractions (10.7%, 12.3%, and 9.7%, respectively). The g−g−g−, ttg+, g+tg+, and g+g−g+ conformers show no significant population, in contrast to ref 14. It is notable that only conformations including a trans orientation of a hydroxyl hydrogen atom show a nonvanishing population if this hydrogen

TABLE 1: Electronic Energy (*E*) and Gibbs Enthalpy (*G*) (298.15 K) Differences with Respect to the Conformer with the Lowest Energy/Enthalpy Value Obtained for the Conformers of AGP without Including Any Solvent Effect (Left-Hand Side) and with Employing the Continuum Model COSMO (Right-Hand Side) in the Chair Conformation[a]

conformer (chair)	ΔE [kJ/mol]	ΔG [kJ/mol]	ΔE [kJ/mol] (COSMO)	ΔG [kJ/mol] (COSMO)
g−g+t	0.00 (36.66)	0.18 (13.29)	0.00 (23.00)	0.06 (9.82)
tg+g+	2.07 (15.89)	0.35 (12.41)	1.33 (13.47)	0.00 (10.06)
tg−g+	2.07 (15.88)	0.37 (12.31)	4.75 (3.38)	3.87 (2.11)
g−g+g−	2.97 (11.05)	0.73 (10.65)	0.78 (16.82)	0.35 (8.74)
g−g+g+	3.55 (8.75)	0.00 (14.30)	5.76 (2.26)	1.66 (5.15)
g+g+g+	4.06 (7.14)	0.97 (9.67)	2.58 (8.12)	0.72 (7.53)
g−g−t	8.71 (1.09)	4.69 (2.16)	4.19 (4.25)	3.77 (2.20)
g−g−g+	9.90 (0.67)	5.43 (1.60)	7.36 (1.18)	3.57 (2.38)
g−g−g−	9.94 (0.66)	4.55 (2.28)	4.75 (3.39)	3.82 (2.16)
tg−g−	9.98 (0.65)	5.36 (1.65)	10.58 (0.32)	5.33 (1.17)
g+g−g+	10.63 (0.50)	4.58 (2.25)	5.29 (2.72)	3.97 (2.03)
ttg+	11.97 (0.29)	3.86 (3.01)	4.35 (3.98)	2.92 (3.10)
g−tg+	12.51 (0.24)	5.13 (1.81)	7.07 (1.33)	3.19 (2.78)
g+tg+	12.56 (0.23)	4.35 (2.47)	4.92 (3.17)	3.05 (2.94)
g−tg−	13.75 (0.14)	4.26 (2.56)	4.42 (3.87)	3.03 (2.96)
g−tt	14.17 (0.12)	4.14 (2.69)	3.79 (4.99)	2.81 (3.24)
tg+t	21.62 (0.01)	4.05 (2.79)	8.78 (0.67)	1.46 (5.58)
g+g+g−	25.57 (0.00)	6.86 (0.90)	10.50 (0.33)	1.55 (5.39)
g+g−g−	28.95 (0.00)	13.38 (0.06)		
g+tg−	31.52 (0.00)	8.18 (0.53)	10.74 (0.30)	3.11 (2.87)
g+g−t	26.63 (0.00)	7.84 (0.60)	10.62 (0.32)	4.62 (1.56)
ttg−			10.29 (0.36)	2.77 (3.29)
tg−t			10.09 (0.39)	5.44 (1.12)
g+tt			10.00 (0.41)	3.06 (2.93)
g+g+t			9.67 (0.47)	1.87 (4.73)
tg+g−			9.45 (0.51)	2.20 (4.14)

[a] The values in brackets give the population in percentage obtained by a Boltzmann distribution (298.15 K).

atom is the H(20) atom, which may be due to favorable hydrogen bonding interactions with the oxygen atom of the ring. For the conformations ttt, ttg−, tg−t, g+tt, g+g+t, and tg+g−, no electronic energy minima were obtained.

The electronic energy differences and the corresponding populations obtained with the COSMO continuum model (compare Table 1) differ from the ones obtained without COSMO (compare Table 1). The most stable conformer is again the g−g+t conformer, although its population is evaluated to be 23% instead of 37%. The g−g+g−, tg+g+, and g+g+g+ are also estimated to be quite abundant. However, the population of tg−g+ is found to be 3% instead of 16% without the continuum model. No energy minimum was found for the g+g−g− and ttt rotamers. The populations obtained with the Gibbs enthalpies at 298.15 K reflect in most cases the results found by the electronic energy differences although the absolute values may differ. Obviously, there is no population with less than 1% contrary to the ones obtained from the electronic energy differences. Furthermore, the tg+t, g+g+g−, g+g+t, and tg+g− conformers are predicted to be higher populated (4%−5%), whereas negligible values were calculated for the populations when considering only the electronic energy differences.

Inspecting the populations evaluated with the electronic energy differences considering only the boat conformers (with COSMO), relatively large populations were calculated for the g+g−t (13%), ttg− (9%), tg+t (8%), g−g−t (7%), and g+tg− (7%) rotamers. The remaining conformers are populated to at least 1%. However, comparing the energies with the ones of the chair conformations, the population of the g+g−t conformer is only 3%, which is in accordance with ref 14, where the populations were calculated from Gibbs energy differences obtained via molecular mechanics simulations. The populations for the tg+t, g−g−t, and g+tg− rotamers lie between 1% and 2%. Employing Gibbs enthalpies, the populations are more equally spread over the different conformers, the smallest one obtained for the g−g+g− conformer with 3%. Interestingly, the largest population is found for the g−g+t conformer (7% instead of 4% derived from the electronic energy differences). The one with the largest population (g+g−t) employing the electronic energy differences is obtained with a population of only 5%.

The electronic energy differences of the conformers containing three water molecules, which solvate the hydroxyl groups in addition to the continuum model, are also given in Table 2. The by far largest populations were obtained for the g−tt (77%) and tg−g+ (18%) rotamers, where the water molecules are oriented in such a way that they can interact with the hydrogen and the oxygen atoms of different hydroxyl groups. The other conformers show negligible populations. We give only the populations evaluated with the Gibbs enthalpies for these conformers, for which no imaginary frequency was found in the calculation because only these represent an energetic minimum. Again, a very high population of 78% is evaluated for the g−tt conformer, followed by the tg+g+,g+g+g+, and g−g+g− conformers with 6%−5%. However, these values must not be overinterpreted since the solvation with only three water molecules is, of course, not sufficient for a complete solvation of the whole molecule.

4.2. Construction of Spectra and Comparison to Experiment. As was shown in the previous section, there is not only one conformer with a considerable population. This implies that the measured ROA spectrum is a superposition of the ROA spectra of certain conformers. The ROA intensities of the different conformers were multiplied by the population fractions calculated from the Gibbs enthalpy differences (indicated in the spectra by "G") or from the electronic energy differences ("E" in the corresponding spectra) (compare section 4.1) for the conformations being considered. These individual ROA intensities were then summed up to generate the full ROA spectrum.

TABLE 2: Electronic Energy (*E*) and Gibbs Enthalpy (*G*) (298.15 K) Differences Compared to the Conformer with the Lowest Electronic Energy/Enthalpy Obtained Employing COSMO for the Conformers of AGP in the Boat (Left-Hand Side) Conformation[a]

conformer	Δ*E* [kJ/mol] (boat) (COSMO)	Δ*G* [kJ/mol] (boat) (COSMO)	Δ*E* [kJ/mol] (chair) (COSMO+expl.solv.)	Δ*G* [kJ/mol] (chair) (COSMO+expl.solv.)
g−g+t	3.10 (3.79)	0.00 (7.05)	11.69 (0.69)	15.74 (0.14)
g−g+g−	6.23 (1.07)	2.54 (2.53)	12.62 (0.47)	6.72 (5.22)
tg+g+	4.27 (2.36)	2.04 (3.09)	12.48 (0.50)	6.64 (5.39)
g+g+g+	5.79 (1.28)	1.25 (4.26)	13.76 (0.30)	6.67 (5.32)
g−tt			0.00 (76.83)	0.00 (78.46)
g−g−t	1.46 (7.33)	1.22 (4.31)	11.31 (0.80)	13.83 (0.30)
ttg+	2.05 (5.78)	0.88 (4.94)	12.24 (0.55)	
g−tg−	2.67 (4.50)	0.90 (4.90)	12.31 (0.53)	13.25 (0.37)
g−g−g−	3.90 (2.74)	1.14 (4.45)	12.66 (0.46)	
tg−g+			3.62 (17.80)	10.60 (1.09)
g+tg+	2.70 (4.46)	0.79 (5.12)	12.65 (0.47)	20.30 (0.02)
g+g−g+	3.09 (3.79)	1.35 (4.09)	13.39 (0.35)	
g−g+g+	7.52 (0.64)	1.40 (4.01)	23.02 (0.01)	8.41 (2.64)
g−tg+	3.78 (2.88)	0.74 (5.23)	24.36 (0.00)	21.20 (0.02)
g−g−g+	4.80 (1.91)	0.92 (4.86)	23.12 (0.01)	16.04 (0.12)
tg+t	1.13 (8.38)	0.60 (5.53)	27.08 (0.00)	18.89 (0.04)
tg+g−	3.29 (3.51)	1.08 (4.56)	27.38 (0.00)	18.90 (0.04)
g+g+t	1.95 (6.02)	0.17 (6.58)	28.51 (0.00)	20.43 (0.02)
g+tt			17.16 (0.08)	12.96 (0.42)
tg−t	2.92 (4.07)	0.88 (4.94)	17.52 (0.07)	
ttg−	0.96 (8.96)	1.68 (3.58)	28.44 (0.00)	
g+g+g−	4.88 (1.85)	1.49 (3.86)	27.84 (0.00)	21.42 (0.01)
g+g−t	0.00 (13.22)	1.00 (4.71)	29.07 (0.00)	
tg−g−			17.52 (0.07)	13.41 (0.35)
g+tg−	1.74 (6.56)	1.17 (4.40)	29.12 (0.00)	26.13 (0.00)
g+g−g−	2.45 (4.92)	2.10 (3.02)	29.59 (0.00)	28.04 (0.00)
ttt			21.37 (0.01)	

[a] the values on the right-hand side correspond to conformers in the chair conformation using COSMO and explicit solvation ("expl.solv.") with three water molecules; the values in brackets give the population in percentage obtained by a Boltzmann distribution (298.15 K).

As a first test, we calculated the ROA spectrum of all chair conformers obtained without solvent effects. Weighting the spectra according to the populations given in Table 1 for the Gibbs enthalpy differences, the spectrum given in Figure 4 was obtained. The experimental spectrum, taken from ref 18, is shown in Figure 6. Since no significant bands were recorded for wave numbers higher than about 1250 cm^{-1}, we compare only the region from 600 to 1250 cm^{-1}. The positive band at about 700 cm^{-1} as well as the negative−positive pattern at around 840 cm^{-1} are found both in the experimental and calculated spectra. In the experimental spectrum, two negative bands are observed at approximately 900 cm^{-1}, which are reproduced in the calculated spectrum although being more separated with a weak negative and positive band in-between. The three positive bands from about 950 to 1050 cm^{-1} in the experimental spectrum are also found in the calculated spectrum. A difference is obvious for the region from 1100 to 1200 cm^{-1} because a positive intensity is calculated at around 1100 cm^{-1}, followed by a negative band at roughly 1170 cm^{-1}, which does not fit to the experimental data with a negative band at around 1100 cm^{-1} and a positive band at about 1150 cm^{-1}. The two intense bands centered at about 1200 cm^{-1} exist in the experimental and in the calculated spectrum. Weighting the here considered conformer spectra by the populations evaluated from the electronic energy differences given in Table 1 does not lead to a better agreement with the experimental spectrum. The corresponding construction of the Raman spectrum is presented in Figure 5. The agreement with the experimental spectrum in Figure 6 is very good although the absolute intensity values differ and the wave numbers are shifted in some cases. The band at roughly 680 cm^{-1} is found in the calculated spectrum as well as the intense band near 810 cm^{-1}. Even the following weak band is reproduced in the calculated spectrum. The positions of the three bands between 850 and 1000 cm^{-1} match the experimental spectrum, yet the peak height differs and they occur at higher wave numbers. The broad band around 1100 cm^{-1} is also found but slightly shifted to lower wave numbers compared to the experimental spectrum. The doublet at about 1200 cm^{-1} also fits the experimental data well.

Incorporating solvent effects, we constructed the ROA spectrum from the spectra of the chair conformers which were calculated with the COSMO continuum model, again with the weighting obtained from the Gibbs enthalpy populations in Table 1. There are some changes, compared to the overlap spectra calculated without the continuum model. The two negative bands around 900 cm^{-1} are better reproduced when comparing to the experimental spectrum. However, the positive and negative bands between about 1100 and 1270 cm^{-1} do not, as was the case also for the spectrum discussed in the previous paragraph, reproduce the negative−positive order of the experimental spectrum. Furthermore, the two positive peaks around 1200 cm^{-1} are plotted as one broadband, which, however, can be modified by choosing another width for the Gaussian band shapes (see the discussion in ref 23).

Taking the boat conformers into account, the overlap spectrum changes slightly. Two weak negative bands are more visible near 1000 cm^{-1}, which does not match the experimental spectrum. In addition, the band at about 1160 cm^{-1} shows a less negative value. However, this peak is not observed in the experimental spectrum at all. Taking the populations obtained from the electronic energy differences in Tables 1 and 2, only minor modifications, e.g., in the 1100−1170 cm^{-1} region, are found but the agreement with the experimental spectrum is not significantly improved. The Raman spectrum evaluated by

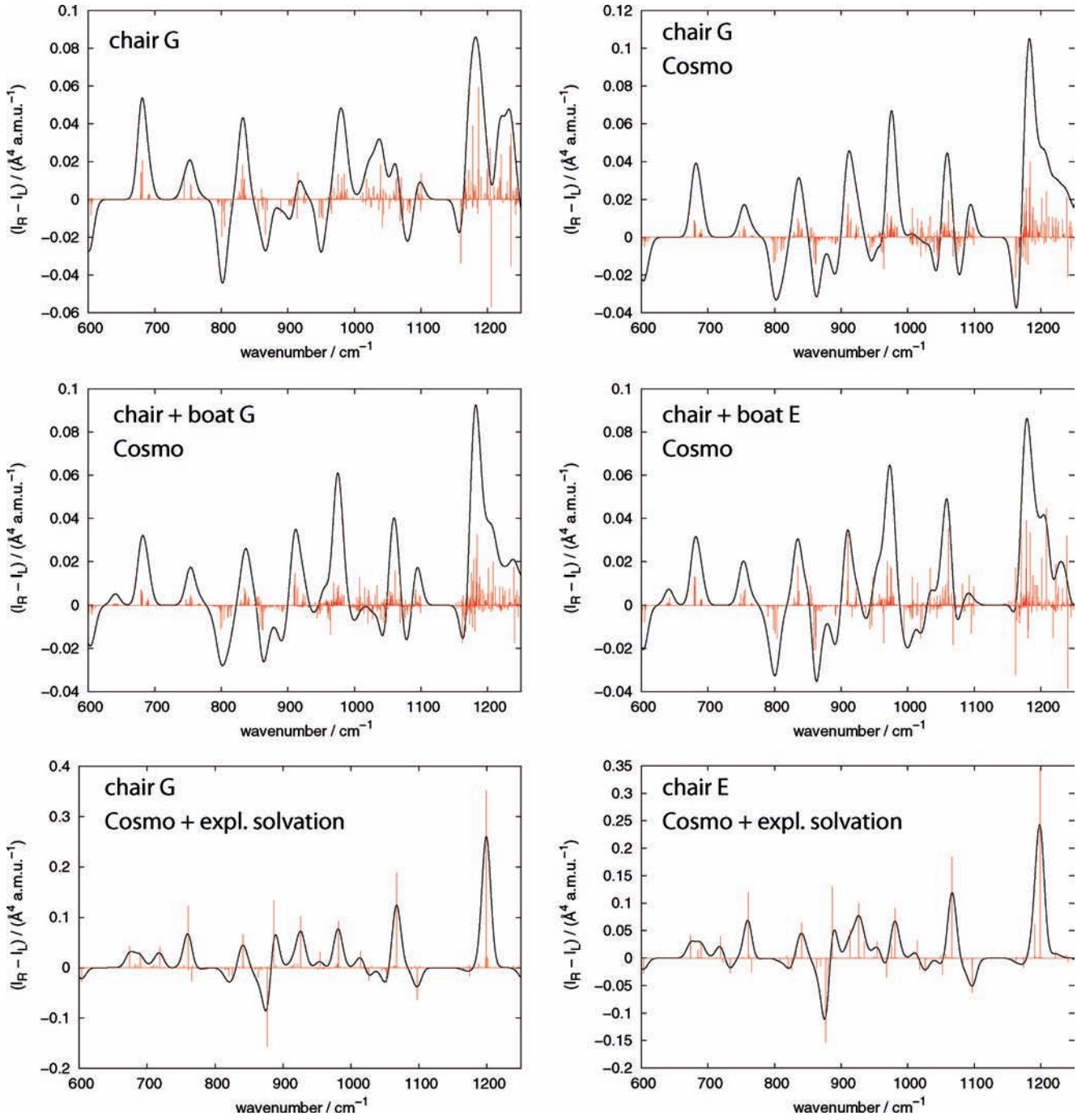

Figure 4. ROA spectra of the backscattering direction (TZVPP/RI/BP86) obtained by overlapping the spectra of all chair conformers (top), calculated without considering solvent effects (left-hand side) and with the continuum model COSMO (right-hand side), and of chair and boat conformers (middle) calculated with COSMO; the spectra on the bottom are obtained from the spectra of the chair conformers and employing COSMO and solvation with water molecules. "E" and "G" indicate weighting according to the populations evaluated from the electronic energy and Gibbs enthalpy differences, respectively; the line spectra were scaled by 0.1.

superimposing the spectra from chair and boat conformers (calculated with COSMO) and weighting according to the Gibbs enthalpy populations (see Tables 1 and 2) does not provide a significant better agreement with the experimental spectrum. Weak bands around 640 and 760 cm^{-1} appear to be too high in comparison with the experimental spectrum. Noteworthy is the small modification in the intensities of the three dominating bands between 850 and 1000 cm^{-1} in the calculated spectrum matching the heights in the experimental spectrum slightly better.

As a final step, the ROA spectrum was constructed from the ROA spectra obtained from the AGP-molecule conformers with three water molecules in addition to the use of the COSMO model. As was shown above, the influence of the spectra of the boat conformers on the overlap spectrum obtained with COSMO was very small, mainly due to their very small populations. We expect that a similar situation may be found for the solvated boat conformers and, therefore, we did not calculate the ROA spectra of the boat rotamers solvated with water molecules. The spectra of the solvated chair conformers were weighted according to the percentages given in Table 2. The spectrum obtained when considering the Gibbs enthalpy differences is presented at the bottom of Figure 4 on the left-hand side and the one taking the electronic energy differences into account on the right-

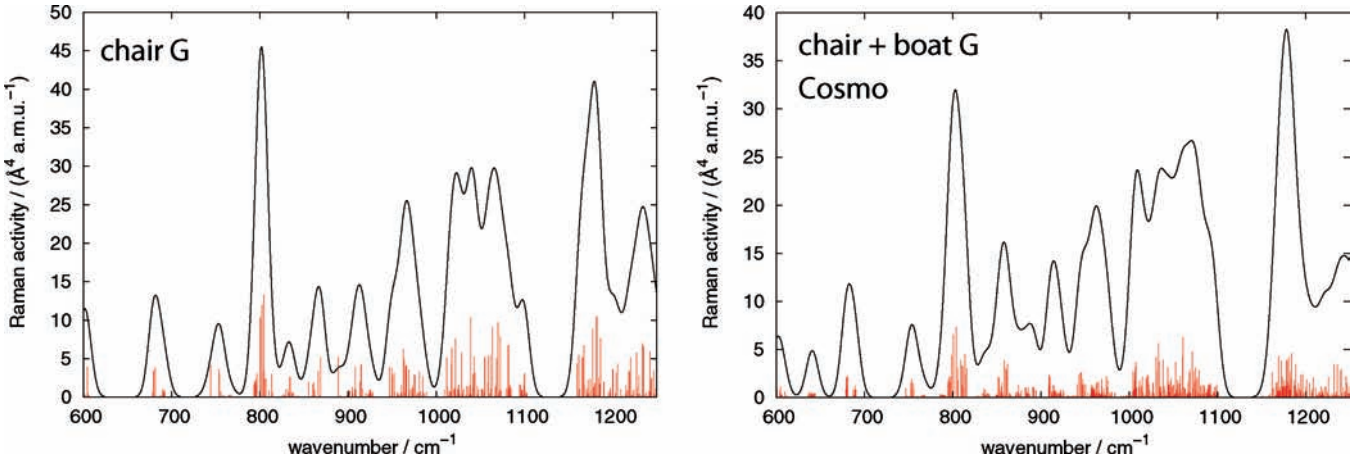

Figure 5. Raman spectra of the backscattering direction (TZVPP/RI/BP86) obtained by overlapping the spectra of all chair conformers calculated without solvent effects (left-hand side) and of chair and boat conformers employing COSMO (right-hand side); "G" indicates weighting according to the populations evaluated with the help of Gibbs enthalpy differences; the line spectra were scaled by 0.1.

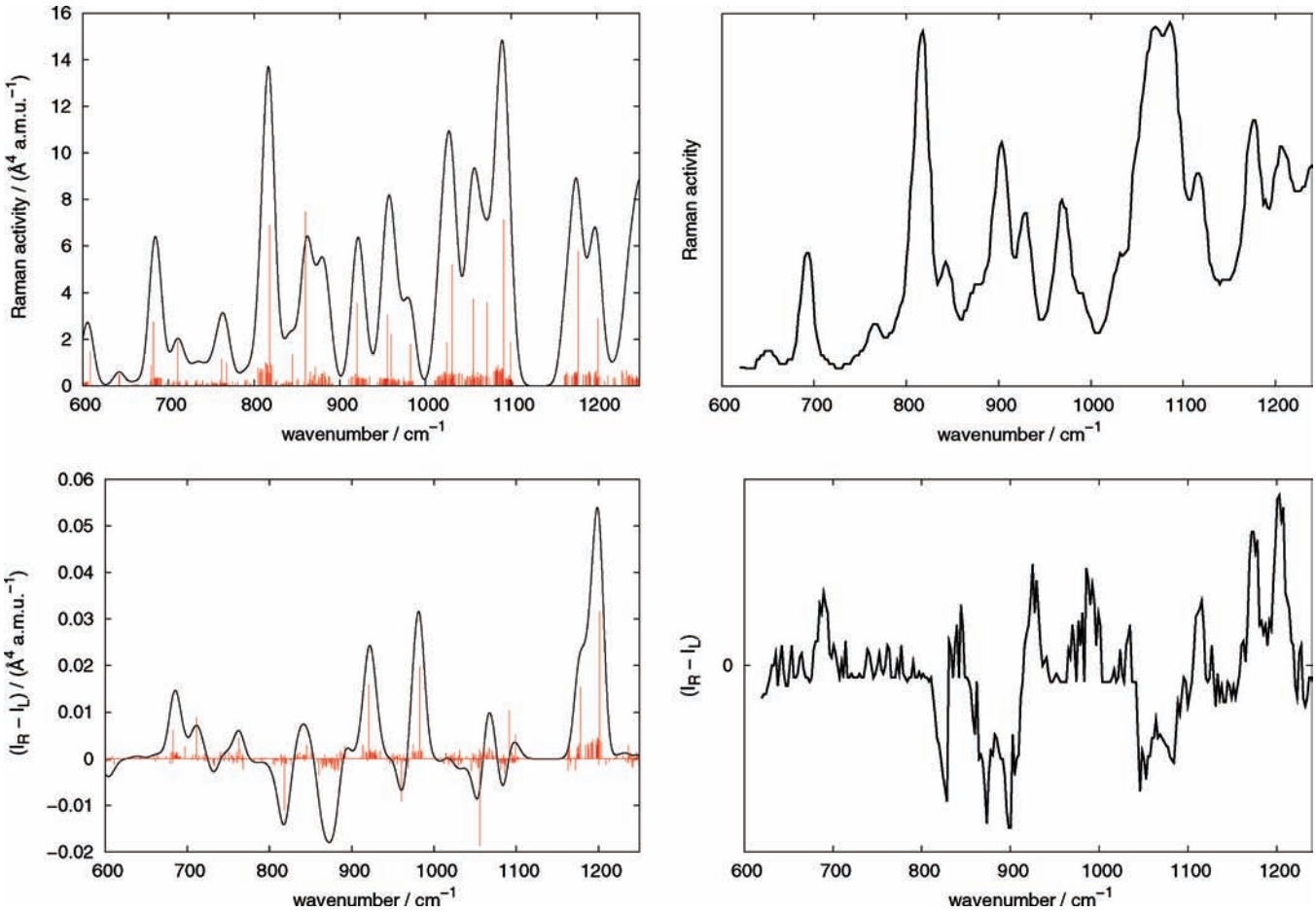

Figure 6. Raman (top) and ROA (bottom) spectra of the backscattering direction (TZVPP/RI/BP86) obtained by overlapping the spectra of all explicitly solvated chair conformers (left-hand side) and the experimental spectra (right-hand side; reproduced from the data provided in ref 18); the line spectra were scaled by 0.1.

hand side. The former provides the most remarkable patterns although a single negative band instead of the doublet around 880 cm^{-1} is found and the following positive band occurs already at wave numbers lower than 900 cm^{-1}. The region from 1050 to 1200 cm^{-1} contains again a strong positive band, followed by a negative one, which does not agree with the negative doublet and the positive band observed in the experimental spectrum. The spectrum evaluated with respect to the populations from the electronic energy differences (see Figure 4 and Table 2) is also a satisfactory approximation to the experimental one. This is in agreement with optical rotation studies, for which the populations evaluated from the electronic energy differences turned out to be a good choice[64] (without considering solvent effects). Since only a couple of conformers show a significant population, we in addition omitted the weighting factors and constructed the spectrum by superimposing the spectra of all chair conformers (see Figure 6). The resulting spectrum is in quite good agreement with the experimental one. The broad negative band around 880 cm^{-1} corresponds to two narrow bands in the experimental spectrum. A

similar result is found for the broad band at approximately 1200 cm^{-1}. The positive bands in the region from 900 to 1050 cm^{-1} are easily visible. One disagreement with the experimental spectrum is again the positive peak between the negative bands around 1070 cm^{-1}, which is not observed in the experimental spectrum. The negative band at roughly 1180 cm^{-1}, which was observed in most of the calculated spectra, does not occur. The analogously constructed Raman spectrum is also given in Figure 6. The agreement with the experimental spectrum is essentially as good as found for the spectra in Figure 5.

5. Summary and Conclusion

We have presented an approach for the calculation of the ROA (and Raman) spectrum of the anhydro sugar AGP. This molecule possesses three hydroxyl groups, which give rise to a variety of rotamers in addition to the chair-boat conformations. Most of the boat conformers were found to be less abundant than the majority of chair conformers. We showed that the change from the chair ($^1C_4$) to the boat ($B_{0,3}$) conformation changes the corresponding ROA intensities significantly. This was also the case for the different rotamers. Modifications of the orientation of the hydrogen atoms of the hydroxyl groups can lead to a large variation in the ROA intensities, showing the great sensitivity of ROA spectroscopy.

In order to include solvent effects, we proceeded stepwise. First, we calculated ROA spectra with the continuum model COSMO, which affects the vibrational frequencies and in this way indirectly the intensities giving rise to only minor alterations of the spectrum compared to the one obtained for the isolated conformers (similar observations have also been described in ref. 61 for Raman spectra). Second, we solvated the molecules in such a way that each hydrogen atom of the three hydroxyl groups interacts with one oxygen atom of a water molecule, which directly leads to a change in Raman and ROA intensities. Calculating the spectra of these microsolvated structures, again embedded in a COSMO environment, resulted in a completely different ROA spectrum, illustrating the large effect on ROA spectra as exerted by the solvent molecules that bind to the solute molecule via weak but directed contacts (hydrogen bonds).

The final spectra were constructed by superimposing spectra of different conformers. The weight of each spectrum was determined by the conformer population which was calculated from the electronic energy or Gibbs enthalpy values. The agreement of the resulting Raman spectrum with the experimental one has already been very good if only the calculations of the chair conformers without any solvent effect were considered. No notable improvement was found if the boat conformers and continuum model solvation effects were included. The situation was different for the ROA spectrum. Considering only the chair conformers and no solvent effects leads to a spectrum that matched the experimental poorly. In contrast to the Raman spectrum, the employment of the continuum model increased the agreement with the experimental spectrum independently of whether the populations obtained from the energies or Gibbs enthalpies were employed. Due to their small populations, the spectra of the boat conformers did not influence the final spectrum strongly. Overlapping the spectra obtained with the explicitly solvated chair conformers led to quite good agreement with the experimental spectrum independently of whether the populations were evaluated from the electronic energy, the Gibbs enthalpies or no weighting was used at all.

The remaining deviations from the experimental spectrum may be removed by a more sophisticated way of including solvent effects. This can, for example, be achieved by a more advanced continuum model.[65] Furthermore, MD calculations can be employed in order to obtain better starting structures for the ROA spectra calculations (for an overview of (traditional) MD calculations regarding hexopyranoses see ref. 66) as was recently done for chiroptical properties.[67] First-principles MD simulations[68,69] as well as quantum-mechanical/molecular-mechanical approaches[70] may be a route to even more accurate calculations of solvent effects on the Raman and ROA spectra of polar molecules and will be investigated in future studies.

Acknowledgment. We thank Prof. K. Ruud for fruitful discussions and valuable comments on the manuscript. This work was supported by the Swiss National Science Foundation (project 200020-121870).

References and Notes

(1) Ĉerný, M. *Adv. Carbohydr. Chem. Biochem.* **2003**, *58*, 121–198.
(2) La Forge, F. B.; Hudson, C. S. *J. Biol. Chem.* **1917**, *30*, 61–77.
(3) Park, Y. J.; Kim, H. S.; Jeffrey, G. A. *Acta Crystallogr.* **1971**, *B27*, 220–227.
(4) Peat, S. *Adv. Carbohydr. Chem.* **1946**, *2*, 37–78.
(5) Carvalho, J. D.; Prins, W.; Schuerch, C. *J. Am. Chem. Soc.* **1959**, *81*, 4054–4058.
(6) Angyal, S. J.; Dawes, K. *Aust. J. Chem.* **1968**, *21*, 2747–2760.
(7) Heyns, K.; Weyer, J. *Liebigs Ann. Chem.* **1968**, *718*, 224–237.
(8) Budêšínský, M.; Trnka, T.; Ĉerný, M. *Collect. Czech. Chem. Commun.* **1970**, *44*, 1949–1964.
(9) Lauterwein, J.; Schulte, J.; Schumacher, M.; Ĉernỳ, M. *Magn. Reson. Chem.* **1992**, *30*, 312–319.
(10) Bonn, G. *J. Carbohydr. Chem.* **1985**, *4*, 405–419.
(11) Ĉerný, M.; Pacák, J.; Stanêk, J. *Chem. Ind.* **1966**, *37*, 1559–1560.
(12) Stevens, E. S. *Carbohydr. Res.* **1993**, *244*, 191–195.
(13) Jeffrey, G. A.; Park, Y. J. *Carbohydr. Res.* **1979**, *74*, 1–5.
(14) Straathof, A. J. J.; Van Estrik, A.; Kieboom, A. P.; Baas, J. M. A.; Van De Graaf, B. *Carbohydr. Res.* **1989**, *194*, 296–299.
(15) Lindberg, K. B. *Acta Chem. Scand. A* **1974**, *28*, 1181–1182.
(16) Barron, L. D.; Boogard, M. P.; Buckingham, A. D. *J. Am. Chem. Soc.* **1973**, *95*, 603–605.
(17) Hug, W.; Kint, S.; Bailey, G.; Scherer, J. R. *J. Am. Chem. Soc.* **1975**, *97*, 5589–5590.
(18) Barron, L. D.; Gargaro, A. R.; Wen, Z. Q. *Carbohydr. Res.* **1991**, *210*, 39–49.
(19) Helgaker, T.; Ruud, K.; Bak, K. L.; Jørgensen, P.; Olsen, J. *Faraday Discuss.* **1994**, *99*, 165–180.
(20) Bouř, P.; Baumruk, V.; Hanzlikovà, J. *Collect. Czech. Chem. Commun.* **1997**, *62*, 1384–1395.
(21) Ruud, K.; Helgaker, T.; Bouř, P. *J. Phys. Chem. A* **2002**, *106*, 7448–7455.
(22) Pecul, M.; Rizzo, A.; Leszczynski, J. *J. Phys. Chem. A* **2002**, *106*, 11008–11016.
(23) Herrmann, C.; Ruud, K.; Reiher, M. *ChemPhysChem* **2006**, *7*, 2189–2196.
(24) Pecul, M.; Ruud, K. *Int. J. Quantum Chem.* **2005**, *104*, 816–829.
(25) Reiher, M.; Liégeois, V.; Ruud, K. *J. Phys. Chem. A* **2005**, *109*, 7567–7574.
(26) Kapitán, J.; Baumruk, V.; Bouř, P. *J. Am. Chem. Soc.* **2006**, *128*, 2438–2443.
(27) Kapitán, J.; Zhu, F.; Hecht, L.; Gardiner, J.; Seebach, D.; Barron, L. D. *Angew. Chem., Int. Ed.* **2008**, *47*, 6392–6394.
(28) Kapitán, J.; Zhu, F.; Hecht, L.; Gardiner, J.; Seebach, D.; Barron, L. D. *Angew. Chem.* **2008**, *120*, 6492–6494.
(29) Pecul, M. *Chem. Phys. Lett.* **2006**, *427*, 166–176.
(30) Liégeois, V.; Ruud, K.; Champagne, B. *J. Chem. Phys.* **2007**, *127*, 204105.
(31) Herrmann, C.; Ruud, K.; Reiher, M. *Chem. Phys.* **2008**, *343*, 200–209.
(32) Luber, S.; Herrmann, C.; Reiher, M. *J. Phys. Chem. B* **2008**, *112*, 2218–2232.
(33) Luber, S.; Reiher, M. *Chem. Phys.* **2008**, *346*, 212–223.
(34) Jacob, C. R.; Luber, S.; Reiher, M. *ChemPhysChem* **2008**, *9*, 2177–2180.
(35) Bell, A. F.; Hecht, L.; Barron, L. D. *J. Raman Spectrosc.* **1993**, *24*, 633–635.
(36) Bell, A. F.; Hecht, L.; Barron, L. D. *J. Am. Chem. Soc.* **1994**, *116*, 5155–5161.
(37) Bell, A. F.; Hecht, L.; Barron, L. D. *J. Raman Spectrosc.* **1995**, *26*, 1071–1074.

(38) Bell, A. F.; Hecht, L.; Barron, L. D. *Spectrochim. Acta Part A* **1995**, *51*, 1367–1378.
(39) Bell, A. F.; Hecht, L.; Barron, L. D. *Chem.—Eur. J.* **1997**, *3*, 1292–1298.
(40) Zhu, F.; Isaacs, N. W.; Hecht, L.; Barron, L. D. *J. Am. Chem. Soc.* **2005**, *127*, 6142–6143.
(41) Zhu, F.; Isaacs, N. W.; Hecht, L.; Trantler, G. E.; Barron, L. D. *Chirality* **2006**, *18*, 103–115.
(42) Macleod, N. A.; Johannessen, C.; Hecht, L.; Barron, L. D.; Simons, J. P. *Int. J. Mass Spectrom.* **2006**, *253*, 193–200. Upon revision of this paper, we became aware of a second theoretical ROA study on gluconic acid anion: Kaminský, J.; Kapitán, J.; Baumruk, V.; Bednárová, L.; Bouř, P. *J. Phys. Chem. A* **2009**, *113*, 3594–3601.
(43) Ahlrichs, R.; Bär, M.; Häser, M.; Horn, H.; Kölmel, C. *Chem. Phys. Lett.* **1989**, *162*, 165–169.
(44) Becke, A. D. *Phys. Rev. A* **1988**, *38*, 3098–3100.
(45) Perdew, J. P. *Phys. Rev. B* **1986**, *33*, 8822–8824.
(46) Schäfer, A.; Huber, C.; Ahlrichs, R. *J. Chem. Phys.* **1994**, *100*, 5829–5835.
(47) Dunning, T. H., Jr. *J. Chem. Phys.* **1989**, *90*, 1007–1023.
(48) Neugebauer, J.; Reiher, M.; Kind, C.; Hess, B. A. *J. Comput. Chem.* **2002**, *23*, 895–910.
(49) Brehm, G.; Reiher, M.; Schneider, S. *J. Phys. Chem. A* **2002**, *106*, 12024–12034.
(50) Neugebauer, J.; Hess, B. A. *J. Chem. Phys.* **2003**, *118*, 7215–7225.
(51) Reiher, M.; Brehm, G.; Schneider, S. *J. Phys. Chem. A* **2004**, *108*, 734–742.
(52) Herrmann, C.; Reiher, M. *Top. Curr. Chem.* **2007**, *268*, 85–132.
(53) Kiewisch, K.; Luber, S.; Neugebauer, J.; Reiher, M. *CHIMIA* **2009**, *63*, 270–274.
(54) Schneider, W.; Thiel, W. *Chem. Phys. Lett.* **1989**, *157*, 367–373.
(55) ftp://ftp.chemie.uni-karlsruhe.de/pub/jbasen.
(56) Klamt, A.; Schüürmann, G. *J. Chem. Soc. Perkin Trans. 2* **1993**, *5*, 799–805.
(57) Kirchner, B.; Reiher, M. *J. Am. Chem. Soc.* **2002**, *124*, 6206–6215.
(58) IUPAC-IUB Joint Commission on Biochemical Nomenclature (JCBN), *Arch. Biochem. Biophys.* **1981**, *207*, 469−472.
(59) Barron, L. D. *Molecular Light Scattering and Optical Activity*, 2nd ed.; Cambridge University Press: Cambridge, 2004.
(60) Hug, W. *Chem. Phys.* **2001**, *264*, 53–69.
(61) Jacob, C. R.; Luber, S.; Reiher, M. *J. Phys. Chem. B* **2009**, *113*, 6558–6573.
(62) Jacob, C. R.; Reiher, M. *J. Chem. Phys.* **2009**, *130*, 084106.
(63) Jacob, C. R.; Luber, S.; Reiher, M. 2009, in preparation.
(64) Grimme, S.; Mück-Lichtenfeld, C. *Chirality* **2008**, *20*, 1009–1015.
(65) Pecul, M.; Lamparska, E.; Cappelli, C.; Frediani, L.; Ruud, K. *J. Phys. Chem. A* **2006**, *110*, 2807–2815.
(66) Kräutler, V.; Müller, M.; Hünenberger, P. H. *Carbohydr. Res.* **2007**, *342*, 2097–2124.
(67) Kundrat, M. D.; Autschbach, J. *J. Chem. Theory Comput.* **2008**, *4*, 1902–1914.
(68) Marx, D.; Hutter, J. Ab Initio Molecular Dynamics: Theory and Implementation. In *Modern Methods and Algorithms of Quantum Chemistry, Proceedings, NIC Series*; Grotendorst, J., Ed.; John von Neumann Institute for Computing: Jülich, 2000; Vol. 3.
(69) Thar, J.; Reckien, W.; Kirchner, B. *Top. Curr. Chem.* **2007**, *268*, 173–290.
(70) Senn, H.-M.; Thiel, W. *Top. Curr. Chem.* **2007**, *268*, 173–290.

JP902828R